# The structure of the 80S ribosome from *Trypanosoma cruzi* reveals unique rRNA components

**Haixiao Gao*, Maximiliano Juri Ayub†, Mariano J. Levin†, and Joachim Frank*‡§**

*Howard Hughes Medical Institute, Health Research, Inc., at the Wadsworth Center, Empire State Plaza, Albany, NY 12201-0509; ‡Department of Biomedical Sciences, State University of New York, Empire State Plaza, Albany, NY 12201-0509; and †Laboratory of Molecular Biology of Chagas Disease (LaBMECh), Instituto de Ingenieria Genetica y Biologia Molecular, National Research Council (CONICET), 1428 Buenos Aires, Argentina

Edited by Thomas A. Steitz, Yale University, New Haven, CT, and approved June 8, 2005 (received for review March 22, 2005)

**We present analysis, by cryo-electron microscopy and single-particle reconstruction, of the structure of the 80S ribosome from *Trypanosoma cruzi*, the kinetoplastid protozoan pathogen that causes Chagas disease. The density map of the *T. cruzi* 80S ribosome shows the phylogenetically conserved eukaryotic rRNA core structure, together with distinctive structural features in both the small and large subunits. Remarkably, a previously undescribed helical structure appears in the small subunit in the vicinity of the mRNA exit channel. We propose that this rRNA structure likely participates in the recruitment of ribosome onto the 5′ end of mRNA, in facilitating and modulating the initiation of translation that is unique to the trypanosomes.**

eukaryote | translation | initiation

The trypanosomatidae family encompasses a group of flagellated protozoans causing a series of severe diseases: *Trypanosoma cruzi*, *Trypanosoma brucei*, and species of *Leishmania*. They have evolved very differently from bacteria, yeast, and animal cells, and have developed unique cellular and genetic pathways. These protozoans are also among those few lower eukaryotic organisms that possess unusually structured mRNAs, as products of a special transsplicing RNA editing mechanism in posttranscription (1–3). As the result of transsplicing, every trypanosome mRNA has 39 identical nucleotides at the 5′ terminus, the so-called spliced leader (SL). Besides the universally conserved 7-methyl guanosine cap, which is linked to the first nucleotide via a 5′-5′ triphosphate bridge, the first four nucleotides of the 39-nt SL are all methylation-modified. This unusually modified cap, known as the cap-4 structure (4–7), is the most highly modified cap structure among all eukaryotic cells.

The functionality of the specially constructed mRNAs in the trypanosome and the reason for their occurrence in only a few organisms are as yet unknown. Counting on the important role of the mRNA 5′ end during eukaryotic translation initiation (8), the SL sequence and its associated cap structure are expected to play a significant part in translation initiation, and possibly to be involved in a unique mechanism of initiation. Indeed, mRNAs processed by transsplicing were found to be translated with higher efficiency than the regularly constructed mRNA, on account of the synergistic cooperation between SL sequence and its associated cap structure (9, 10). There is increasing evidence in biochemical studies for direct interactions between ribosome and SL sequence/cap structure through complementary base pairing (11–13). In kinetoplastid *Leishmania*, the cap-4 structure and the first two thirds of the SL sequence have been found to be critical for the association of mRNAs with polysomes (13).

Here, we have used cryo-EM to obtain the structure of the *T. cruzi* 80S ribosome. In comparison with ribosomal structures from other species, the density map of *T. cruzi* 80S ribosome shows the presence of unusual structural components, related to large expansion segments in the rRNA secondary structure. We postulate that these unusual ribosomal components are involved in the unique mechanism of translation initiation in trypanosomes.

## Materials and Methods

**Purification of the *T. cruzi* 80S Ribosome.** Ribosomes were purified from epimastigotes of *T. cruzi* according to the protocol described by Gomez *et al.* (14). All ribosome purification steps were performed at 4°C in the presence of protease inhibitors. The parasites were disrupted in SKS (0.25 M sucrose/5 mM KCl) supplemented with 0.25% of deoxycholate. The homogenate was centrifuged at 1,000 × *g* for 10 min. The supernatant (SN) was repeatedly centrifuged at 12,000 × *g* for 20 min until no pellet was detected. The SN was centrifuged at 105,000 × *g* for 2 h, the pellet was resuspended in buffer I (20 mM Tris·HCl, pH 7.5/100 mM $MgCl_2$/500 mM ammonium acetate/5 mM 2-mercaptoethanol). Afterward, the suspension was clarified several times by centrifugation at 12,000 × *g* for 10 min until no pellet was evident. The SN was loaded on a two-layer discontinuous sucrose gradient formed by a bottom 40% (wt/vol) sucrose solution and a top 20% (wt/vol) sucrose layer. The sample was centrifuged at 105,000 × *g* for 18 h. The translucent pellet was resuspended in buffer II (10 mM Tris·HCl, pH 7.5/12.5 mM $MgCl_2$/80 mM KCl/5 mM 2-mercaptoethanol) and diluted in buffer II. Samples were frozen and stored at −80°C.

**Cryo-EM and Image Processing.** Buffer solutions containing *T. cruzi* 80S ribosome with final concentration of 32 nM were applied to cryo-EM grids at 4°C following the standard procedure using the Vitrobot (FEI, Eindhoven, The Netherlands). A total of 173 micrographs were recorded in a defocus range between 1.0 and 3.3 $\mu$m on a Philips Tecnai F20 electron microscope at 200 kV with a calibrated magnification of 49,650, under low-dose conditions (18 $e^-/Å^2$). The micrographs were digitized on a Zeiss Imaging scanner (Z/I Imaging, Huntsville, AL) with a step size of 14 $\mu$m, corresponding to a pixel size of 2.82 Å on the object scale. After evaluation of drift, astigmatism, and the presence of Thon rings in the power spectrum of each micrograph, 161 good micrographs were selected and divided into 31 defocus groups. Ribosomal particles were selected from these micrographs through three steps: preliminary automated selection, manual verification, and selection based on the size of the cross-correlation coefficient with a template. A total of 53,505 particles were obtained and subjected to the single particle reconstruction. To start, two separate reconstructions were performed on a small dataset of *T. cruzi* 80S ribosome, based on two different reference volumes (80S ribosome from *Thermomyces lanuginosus* and *Saccharomyces cerevisiae*) for projection matching. The two reconstructed volumes were compared and found to be highly consistent in terms of the new structural features.

This paper was submitted directly (Track II) to the PNAS office.

Freely available online through the PNAS open access option.

Abbreviations: SL, spliced leader; CP, central protuberance; ES, expansion segment; cryo-EM, cryo-electron microscopy.

§To whom correspondence should be addressed. E-mail: joachim@wadsworth.org.

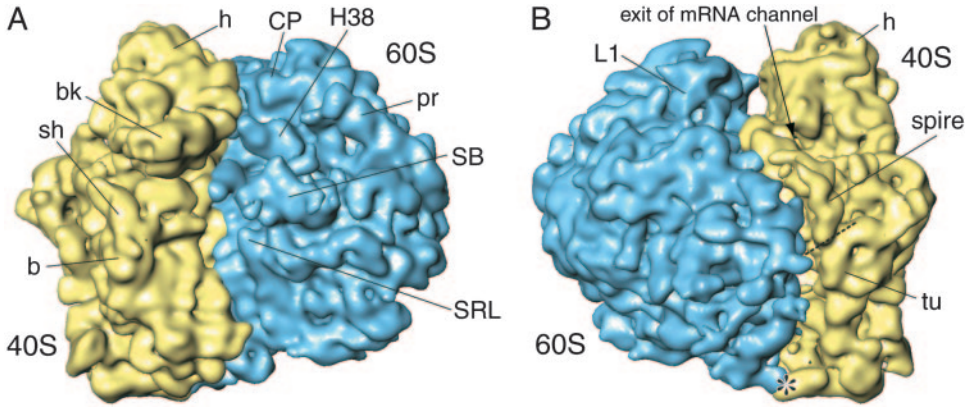


**Fig. 1.** The 12-Å resolution cryo-EM density map of the 80S ribosome from *T. cruzi*. The density map is shown in two side views of the 80S ribosome. The 40S subunit is in yellow and the 60S subunit in blue. Landmarks for the 40S subunit: h, head; bk, beak; sh, shoulder; b, body; tu, turret; landmarks for the 60S subunit: CP, central protuberance; H38, helix 38; SB, stalk base; pr, prong; SRL, sarcin–ricin loop; L1, L1 stalk. The dashed line defines the spire of the turret. The asterisk marks the previously undescribed connection between the small and large ribosomal subunits.

One of the newly reconstructed volumes was then used as reference volume applied to the entire data set for the final reconstruction. The final resolution of the CTF-corrected volume was estimated by the Fourier Shell Correlation criterion with a cutoff value of 0.5. The falloff of the Fourier amplitudes toward higher spatial frequencies was corrected as described (15), using the x-ray solution scattering intensity distribution of the *Escherichia coli* 70S ribosome. RNA and protein components were computationally separated using a method (16) based on the differences in the density distribution of RNA and proteins, taking into account the molecular masses and RNA contiguity constraints.

All of the steps of image processing were performed by using the SPIDER package (17). The atomic RNA core structure was fitted as rigid body into the EM density map, except that the L1 stalk region was manually docked as a separated rigid body using O (18). The figures were prepared by using IRIS EXPLORER (Numerical Algorithms Group, Downers Grove, IL) and the CHIMERA package (19).

## Results

Using the cryo-EM technique and the single-particle reconstruction method (20), a density map of the *T. cruzi* 80S ribosome with a resolution of 12 Å was reconstructed from purified ribosomal particles. Considering the relatively low total number of particles used in the reconstruction, such resolution indicates that the ribosomal particles in the preparation are highly homogenous. The overall structure of the *T. cruzi* 80S ribosome exhibits well defined small (40S) and large (60S) subunits, in keeping with the feature fundamentally and evolutionally conserved among eukaryotic ribosomes (Fig. 1). Landmark characteristics of the typical ribosome structure are clearly identified in the density map. Compared with the eukaryotic 80S ribosome from yeast, both the small and large ribosomal subunits from *T. cruzi* are larger (1.3 times in volume), mostly on account of the size increments of the ribosomal RNA molecules, with the *T. cruzi* rRNAs [18S rRNA: 2,315 nt (GenBank accession no. AF245382); 28S rRNA: 4,151 nt (www.genedb.org)] being one-fifth larger than the yeast rRNA (18S rRNA: 1,798 nt; 25S rRNA: 3,392 nt), in terms of the total number of nucleotides.

Superposition of the density map of the *T. cruzi* 80S ribosome and the model of the rRNA core structure built on the basis of the cryo-EM map for yeast (21) produces a good fit of the morphological features, indicating that this microorganism possesses the phylogenetically conserved eukaryotic rRNA core structure. As shown in Fig. 2, the spatial ribosomal configuration formed by rRNA core structure is preserved as indicated by the well fitted known RNA components, such as helix 44 from the small subunit and helix 69 from the large subunit.

In terms of the ribosomal proteins, sequence analysis using BLAST search indicates that almost all yeast ribosomal proteins have counterparts in *T. cruzi* (except for L41e and S31), with sequence identities varying between 30% and 70%. Surprisingly, comparison of the density maps of the 40S ribosomal subunits from *T. cruzi* and yeast reveals that RACK1, a large scaffold protein in the head of the 40S subunit is absent from the *T. cruzi* ribosome (Fig. 3). Recently identified as a ribosomal protein by mass spectroscopy (22) and cryo-EM (23), RACK1 is a constituent of all eukaryotic ribosomes visualized by cryo-EM thus far, and apparently plays a direct role in the regulation of eukaryotic translation initiation through the recruitment of protein kinase C (23). Because data mining indicates that a homolog of the RACK1 gene is present in the *T. cruzi* genome, the absence of RACK1 from the *T. cruzi* 80S ribosome revealed by our study might be a reflection of an earlier stage of eukaryotic evolution.

Although the *T. cruzi* 80S ribosome possesses common ribosomal features, it exhibits many distinctive structural features in both the small and large subunits. Compared with prokaryotic and other eukaryotic ribosomes, the *T. cruzi* ribosomal 40S subunit appears expanded, due to the addition of a large piece of density adjacent to the platform region (Fig. 3). As indicated in the secondary structure of the *T. cruzi* 18S rRNA (Fig. 4), this extra density must be attributed to two large expansion segments in domain II of the 18S rRNA, ES6 and ES7, designated as insertions of helices 21 and 26. These are the two largest expansion segments in the *T. cruzi* 18S rRNA, involving 504 and 147 nucleotides, respectively.

Part of ES6/ES7 makes up a large helical structure (which we term the "turret"), located at the most lateral side of the 40S subunit (Fig. 4). The turret measures 205 Å in length, thus forming the longest helical structure ever observed in a ribosome. The upper end of the turret appears as a sharp, freestanding spiral of 50 Å in length, which we term "spire," apposed to the exit of the mRNA channel. The distance between the spire and the mRNA exit is ≈130 Å. The lower portion of the turret extends all of the way to the bottom of the 40S subunit. At its lower end, it bends by almost 90° and forms a bridge with the 60S subunit (Fig. 1). This is a unique type of connection between the small and large subunits, as compared with all other ribosomal

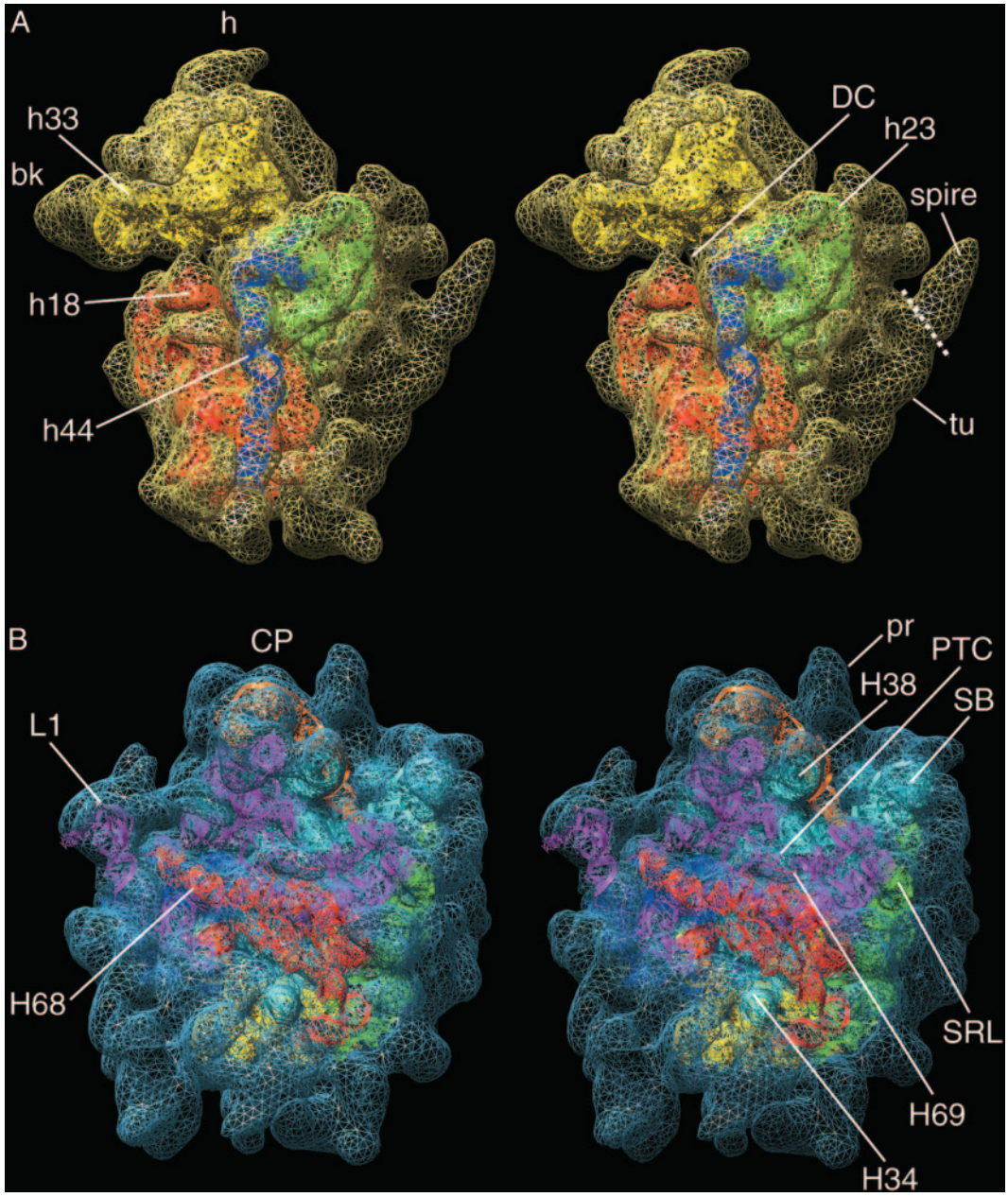


**Fig. 2.** Stereoviews of the conserved rRNA core structure in 40S (*A*) and 60S (*B*) ribosomal subunits from *T. cruzi*. The density maps of the 40S and 60S ribosomal subunits are represented in wire mesh. The atomic structures were directly adopted from the rRNA core structure from yeast (Protein Data Bank ID codes 1S1H and 1S1I). Color codes for the conserved rRNA core in the small subunit: domain I, red; domain II, green; domain III, yellow; domain IV, blue. Color codes for the conserved rRNA core in the large subunit: domain I, blue; domain II, cyan; domain III, yellow; domain IV, red; domain V, magenta; domain VI, green; 5S RNA, orange. h, head; bk, beak; tu, turret; h44, helix 44; h33, helix 33; h18, helix 18; h23, helix 23; DC, decoding center; CP, central protuberance; L1, L1 stalk; pr, prong; SB, stalk base; PTC, peptidyl-transferase center; SRL, sarcin–ricin loop; H34, helix 34; H38, helix 38; H68, helix 68; H69, helix 69.

structures investigated to date (24). Apart from the turret, the extra density in the 40S subunit also includes several small helical structures as part of ES6 and ES7. These helical structures observed in our density map are in accordance with the comparative analysis result based on ES6 sequences from >3,000 eukaryotes, in which several helices were identified only from kinetoplatida (25).

Besides the expansion segments ES6 and ES7, which are related to the turret structure and its subsidiaries, *T. cruzi* 18S rRNA has four additional small expansion segments, designated as ES3, ES9, ES10, and ES12, located in domains I, III, and IV of the 18S rRNA, respectively. Similarly, all of these small expansion segments are found to be associated with the unaccounted density in the *T. cruzi* 40S ribosomal subunit (Fig. 4). ES12 is located in the long penultimate helix (helix 44), and results in the helix 44 in *T. cruzi* (113 nt) being longer than in *E. coli* (103 nt), but shorter than in yeast (129 nt). Consistent with these variations in length, the span of the density attributable to helix 44 in the *T. cruzi* ribosome also has an intermediate position between *E. coli* and yeast. ES3, ES9, and ES10 are located near helices 9, 39, and 41, respectively, and are associated with three small masses in the density map of the 40S ribosomal subunit, one at the bottom of the 40S ribosomal subunit, the other two in the head region.

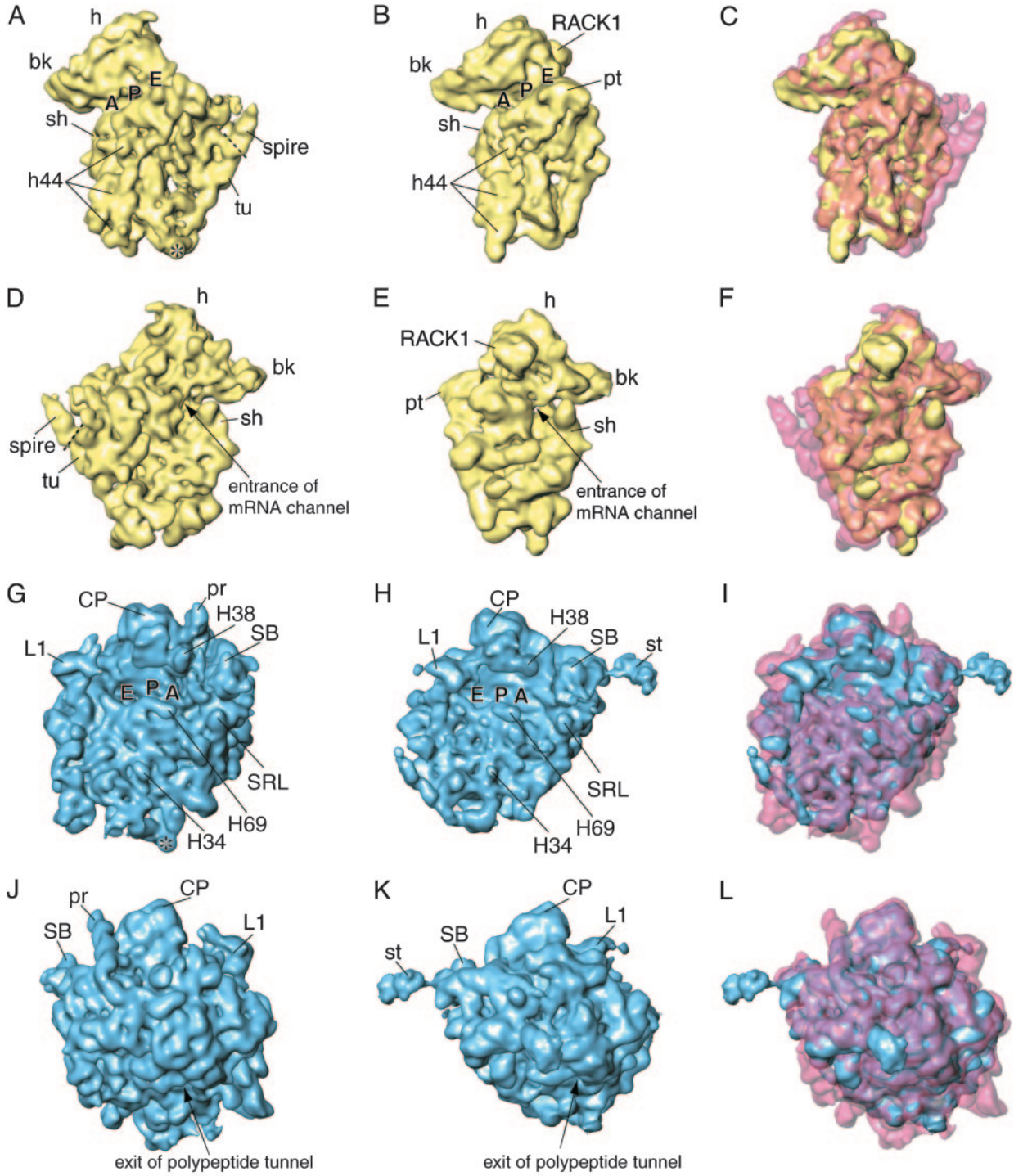


**Fig. 3.** Structural comparison of the ribosomal subunits from *T. cruzi* and yeast (*S. cerevisiae*). (*A* and *B*) Intersubunit view of the 40S subunits. (*D* and *E*) Solvent side view of the 40S subunits. (*C* and *F*) Superposition of the two 40S subunits (*T. cruzi* 40S is in semitransparent red, and yeast 40S in solid yellow). (*G* and *H*) Intersubunit view of the 60S subunits. (*J* and *K*) Solvent side view of the 60S subunits. (*I* and *L*) Superposition of the two 60S subunits (*T. cruzi* 60S is in semitransparent red, and yeast 60S in solid blue). RACK1, protein RACK1; st, P-protein stalk; A, aminoacyl site; P, peptidyl site; E, exit site. Other landmarks are the same as introduced in Fig. 2.

As to the large subunit, besides the common occurrence of the central protuberance (CP), L1 stalk, and stalk base of P proteins, as well as the conserved rRNA core structure, the *T. cruzi* 60S subunit contains several large extra densities located at its periphery, compared with the large ribosomal subunit in yeast (Fig. 3). Although the secondary structure of the *T. cruzi* rRNAs in the 60S subunit is not available, the locations of most of the observed extra densities are consistent with the general locations of the rRNA expansion segments, which are, as a rule, at the surface of the eukaryotic ribosomes (26). Among all of the extra densities, there is a large helical structure ("prong") located between the CP and helix 38, in the back of the 60S subunit (Figs. 1 and 3). Interestingly, a similar feature was only reported in the structure of the human ribosome, but

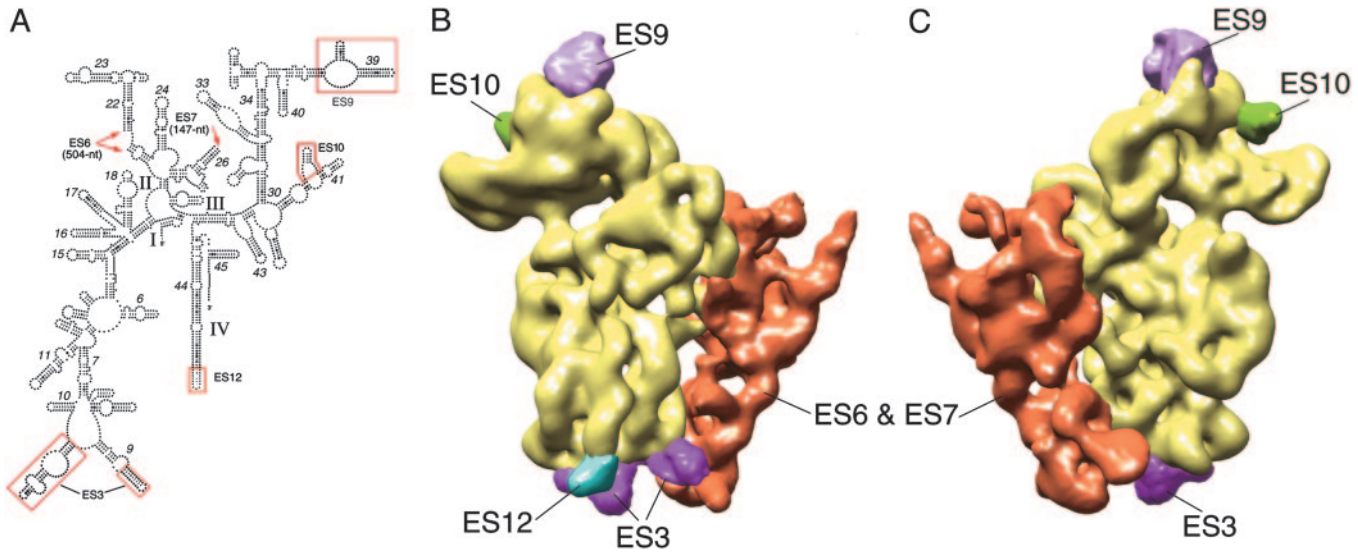


**Fig. 4.** RNA in the *T. cruzi* 40S ribosomal subunit. (*A*) Secondary structure diagram of the *T. cruzi* 18S rRNA (www.rna.icmb.utexas.edu). The expansion segments are marked by using the nomenclature of Gerbi (26). The regions of ES6 and ES7 are indicted by arrows and the number of encompassed nucleotides. (*B* and *C*) RNA partition of the *T. cruzi* 40S ribosomal subunit as viewed from intersubunit side and solvent side. The conserved rRNA core is rendered in yellow. The expansion segments are highlighted: ES6 and ES7, orange; ES3, dark purple; ES9, light purple; ES10, green; ES12, cyan.

not in yeast and bacterial ribosomes (27). Morphological comparison of the 60S ribosomal subunit from *T. cruzi* with those from yeast and other higher eukaryotes reveals that the *T. cruzi* 60S ribosomal subunit does not possess the universal eukaryotic feature as a planar surface near the exit site of polypeptide (24). Instead, the 60S ribosomal subunit from *T. cruzi* presents a shape that is similar to those from bacteria (Fig. 5, which is published as supporting information on the PNAS web site).

In contrast to the conserved eukaryotic rRNA core structure, the location of the L1 stalk in *T. cruzi*, which is on one side of the CP, does not match either of the two reported positions in yeast, known as the "in position" and "out position," in relation to the ratchet-like subunit rearrangement. Instead, the L1 stalk in *T. cruzi* takes an in-between position, possibly due to its high mobility. On the other side of the CP, the P protein stalk is not visible in the density map of the *T. cruzi* 60S ribosomal subunit, whereas Western blots of the ribosome preparation using monoclonal antibodies against P proteins (P0/P1/P2) showed that these proteins were present (see Fig. 6, which is published as supporting information on the PNAS web site). As homologs of the bacterial moiety $L10/(L7/L12)_4$, P proteins are known to be very flexible, and the absence of a stalk in the current EM density map is likely due to the lack of stabilization through additional ligand binding (28).

## Discussion

Structural analysis of the 80S ribosome from *T. cruzi* may be of importance in detecting specific structures necessary for the process of translation of this pathogenic microorganism. Our cryo-EM result shows that one of the most notable structural features in the *T. cruzi* 80S ribosome is associated with the small subunit, as a turret structure forming a large helix with its upper end located in the vicinity of the mRNA exit channel. A comparison of the available secondary structures of the 18S rRNA among eukaryotes (29) indicates that the large expansion segments ES6 and ES7 identified to be associated with the turret structure and its subsidiaries only exist in trypanosomes, where they occur with highly conserved sequence and size (current data available for *T. cruzi*, *T. brucei*, and *L. major*, www.rna.icmb.utexas.edu). On the other hand, the 39-nt SL sequence and its associated cap structure are also highly conserved in these trypanosomes (Fig. 7, which is published as supporting information on the PNAS web site). Thirty of the 39 nucleotides in their SL sequence are identical, including the modified first four nucleotides that compose the cap-4 structure. The unique features of the *T. cruzi* ribosomal components found in our study, along with the unusually structured mRNA conserved among known trypanosomes, suggest the existence of a unique interaction between the trypanosomal ribosome and the mRNA.

In eukaryotic translation initiation, the overwhelming majority of the mRNAs recruit the ribosomal 40S subunit through their 5′-end cap, and a number of initiation factors, including eIF4E, eIF4G, and eIF4A, a process known as the cap-dependent initiation (30). A recent study of the cap-binding protein eIF4E from trypanosome showed that eIF4E in trypanosome has much lower binding affinity with the cap-4 structure, compared to the binding affinity of eIF4E in mouse with monomethylated cap (31). Furthermore, the detected cellular level of eIF4E also appears lower than that required for conducting translation sufficiently (32). In line with these findings of the eccentric behavior of eIF4E in the trypanosome, and the unusually structured mRNA 5′-end conserved among trypanosomes, we propose that the turret structure found in the *T. cruzi* 40S ribosomal subunit may be involved in the translation initiation process in *T. cruzi*.

In the absence of a tertiary structure model related to the turret structure, a legitimate guess would be that the spire region of the turret may be a target for direct interaction with the SL sequence and cap-4 structure at the 5′ end of mRNA. At the free end of the turret structure, the conformation of the spire would allow a certain freedom of movement during the interaction with mRNA. Although a direct sequence scan in ES6 and ES7 does not reveal the nucleotides that form the Watson–Crick base pairs with the cap-4, it is possible that some nucleotides in the 39-nt SL sequence are involved in the base pairing. In addition, the SL sequence itself might be recognized by the turret, perhaps by folding into a specific structure similar to a viral internal ribosome entry site sequence (33), which forms direct RNA–ribosome contacts to initiate translation. A case in point is that the 39-nt spliced leader would fit

the 130-Å distance between the spire and the mRNA exit without being fully extended. In the absence of additional evidence, we cannot rule out other possibilities, e.g., that the turret may represent a special platform for binding distinct initiation factors unique to the trypanosomes or that it may substitute for some initiation factors in trypanosome.

The absence of RACK1 from the small subunit of the *T. cruzi* ribosome may also be involved in defining the very specific nature of translation initiation in these parasite cells. It is conceivable that all protozoan species of the Euglenozoa group, including free living species that possess mRNA processed by transsplicing, share the special ribosomal component observed here, as well as a unique mechanism of translation initiation.

We thank Michael Watters for assisting us with the illustrations. This work was supported by the Howard Hughes Medical Institute (HHMI), National Institutes of Health Grants GM29169 and RR01219 and grants from the National Science Foundation (to J.F.), WHO/Special Program for Research and Training in Tropical Diseases (South–South Initiative project A20363), Fondo Nacional de Investigacion Científica y Tecnològica–Argentinean National Agency for Science and Technology, and the University of Buenos Aires, Buenos Aires, Argentina (to M.J.L.). In addition, M.J.L. was supported by an International Research Scholar grant from HHMI.

1. Walder, J. A., Eder, P. S., Engman, D. M., Brentano, S. T., Walder, R. Y., Knutzon, D. S., Dorfman, D. M. & Donelson, J. E. (1986) *Science* **233,** 569–571.
2. Murphy, W. J., Watkins, K. P. & Agabian, N. (1986) *Cell* **47,** 517–525.
3. Sutton, R. E. & Boothroyd, J. C. (1986) *Cell* **47,** 527–535.
4. Perry, K. L., Watkins, K. P. & Agabian, N. (1987) *Proc. Natl. Acad. Sci. USA* **84,** 8190–8194.
5. Freistadt, M. S., Cross, G. A. & Robertson, H. D. (1988) *J. Biol. Chem.* **263,** 15071–15075.
6. Bangs, J. D., Crain, P. F., Hashizume, T., McCloskey, J. A. & Boothroyd, J. C. (1992) *J. Biol. Chem.* **267,** 9805–9815.
7. Lewdorowicz, M., Yoffe, Y., Zuberek, J., Jemielity, J., Stepinski, J., Kierzek, R., Stolarski, R., Shapira, M. & Darzynkiewicz, E. (2004) *RNA* **10,** 1469–1478.
8. Preiss, T. & Hentze, M. W. (2003) *BioEssays* **25,** 1201–1211.
9. Maroney, P. A., Denker, J. A., Darzynkiewicz, E., Laneve, R. & Nilsen, T. W. (1995) *RNA* **1,** 714–723.
10. Lall, S., Friedmann, C. C., Jankowska-Anyszka, M., Stepinksi, J., Darzynkiewicz, E. & Davis, R. E. (2004) *J. Biol. Chem.* **279,** 45573–45585.
11. Aline, R. F., Jr., Scholler, J. K. & Stuart, K. (1989) *Mol. Biochem. Parasitol.* **32,** 169–178.
12. Liou, R. F. & Blumenthal, T. (1990) *Mol. Cell. Biol.* **10,** 1764–1768.
13. Zeiner, G. M., Sturm, N. R. & Campbell, D. A. (2003) *J. Biol. Chem.* **278,** 38269–38275.
14. Gomez, E. B., Medina, G., Ballesta, J. P. G., Levin, M. J. & Tellez-Inon, M. T. (2001) *Int. J. Parasitol.* **31,** 1032–1039.
15. Gabashvili, I. S., Agrawal, R. K., Spahn, C. M. T., Grassucci, R. A., Frank, J. & Penczek, P. (2000) *Cell* **100,** 537–549.
16. Spahn, C. M. T., Penczek, P., Leith, A. & Frank, J. (2000) *Structure (London)* **8,** 937–948.
17. Frank, J., Radermacher, M., Penczek, P., Zhu, J., Li, Y., Ladjadj, M. & Leith, A. (1996) *J. Struct. Biol.* **116,** 190–199.
18. Jones, T. A., Zhou, J. Y., Cowan, S. W. & Kjeldgaard, M. (1991) *Acta Crystallogr. A* **47,** 110–119.
19. Pettersen, E. F., Goddard, T. D., Huang, C. C., Couch, G. S., Greenblatt, D. M., Meng, E. C. & Ferrin, T. E. (2004) *J. Comput. Chem.* **25,** 1605–1612.
20. Frank, J. (1996) *Three-Dimensional Electron Microscopy of Macromolecular Assemblies* (Academic, New York).
21. Spahn, C. M. T., Gomez-Lorenzo, M. G., Grassucci, G. A., Jorgensen, R., Andersen, G. R., Beckmann, R., Penczek, P. A., Ballesta, J. P. G. & Frank, J. (2004) *EMBO J.* **23,** 1008–1019.
22. Link, A. J., Eng, J., Schieltz, D. M., Carmack, E., Mize, G. J., Morris, D. R., Garvik, B. M. & Yates, J. R., III (1999) *Nat. Biotechnol.* **17,** 676–682.
23. Sengupta, J., Nilsson, J., Gursky, R., Spahn, C. M. T., Nissen, P. & Frank, J. (2004) *Nat. Struct. Mol. Biol.* **11,** 957–962.
24. Frank, J. (2003) *Genome Biol.* **4,** 237.
25. Wuyts, J., De Rijk, P., Van de Peer, Y., Pison, G., Rousseeuw, P. & De Wachter, R. (2000) *Nucleic Acids Res.* **28,** 4698–4708.
26. Gerbi, S. A. (1996) in *Ribosomal RNA. Structure, Evolution, Processing, and Function in Protein Synthesis*, eds. Zimmermann, R. A. & Dahlberg, A. E. (CRC Press, New York), pp. 71–87.
27. Spahn, C. M. T., Jan, E., Mulder, A., Grassucci, R. A., Sarnow, P. & Frank, J. (2004) *Cell* **118,** 465–475.
28. Gomez-Lorenzo, M. G., Spahn, C. M. T., Agrawal, R. K., Grassucci, R. A., Penczek, P., Chakraburtty, K., Ballesta, J. P. G., Lavandera, J. L., Garcia-Bustos, J. F. & Frank, J. (2000) *EMBO J.* **19,** 2710–2718.
29. Cannone, J. J., Subramanian, S., Schnare, M. N., Collett, J. R., D'Souza, L. M., Du, Y., Feng, B., Lin, N., Madabusi, L. V., Muller, K. M., *et al.* (2002) *BMC Bioinformatics* **3,** 2.
30. Kapp, L. D. & Lorsch, J. R. (2004) *Annu. Rev. Biochem.* **73,** 657–704.
31. Yoffe, Y., Zuberek, J., Lewdorowicz, M., Zeira, Z., Keasar, C., Orr-Dahan, I., Jankowska-Anyszka, M., Stepinski, J., Darzynkiewicz, E. & Shapira, M. (2004) *RNA* **10,** 1764–1775.
32. Dhalia, R., Reis, C. R. S., Freire, E. R., Rocha, P. O., Katz, R., Muniz, J. R. C., Standart, N. & de Melo Neto, O. P. (2005) *Mol. Biochem. Parasitol.* **140,** 23–41.
33. Hellen, C. U. T. & Sarnow, P. (2001) *Genes Dev.* **15,** 1593–1612.